

PERTURBING SPANWISE MODES IN TURBULENT BOUNDARY LAYERS

Shaokai Zheng

Department of Aerospace Engineering and Mechanics
University of Minnesota, Minneapolis, MN, 55455, USA
zheng250@umn.edu

Ellen K. Longmire

Department of Aerospace Engineering and Mechanics
University of Minnesota, Minneapolis, MN, 55455, USA
longmire@aem.umn.edu

ABSTRACT

A single spanwise array of cylinders was used to perturb a zero pressure gradient turbulent boundary layer ($Re_\tau=2500$). The cylinder height was $H/\delta=0.2$ ($H^+=500$) with aspect ratio (height/diameter) of $AR=4$, and four cases were studied with cylinder spacing from 0.2δ to 0.8δ . Streamwise-spanwise planes were measured by particle image velocimetry (PIV) up to 7δ downstream at a wall-normal location of $z^+=300$. The 0.6δ case, which matched the dominant spanwise mode in the unperturbed flow, showed the most stable downstream organization which persisted beyond 7δ . The cylinders were observed to sometimes enhance the organization of existing packets and to generally redirect packets into the spanwise location midway between cylinders. Approaching packets lost their organization immediately downstream of the 0.2δ array but regained it downstream, suggesting that the outer layer organization propagated inward into the log region.

INTRODUCTION AND MOTIVATION

Since vortex packets are believed to be a key self-sustaining mechanism in turbulent boundary layers, it may be possible to control boundary layer behavior by manipulating these coherent structures. Since the vortex packets are often associated with strong Q2 ejection events (Adrian *et al.*, 2000), creating long low-momentum regions (LMRs) in the streamwise direction (Tomkins & Adrian, 2003), the features of these LMRs will be used to discuss the physics of packets.

Packets have been observed to occur frequently in the logarithmic region of turbulent boundary layers, such that they are well aligned with the underlying surface (Ganapathisubramani *et al.*, 2003; Elsinga *et al.*, 2007; Lee & Sung, 2011). As this region is also associated with significant energy and wall-normal transport, it is of particular interest in the current investigation. Large scale packets in the logarithmic and outer layers have also been noted to make a significant imprint on the near wall region, seeming to modulate the small scale events at the wall (Hutchins & Marusic, 2007). Additional studies of the packet features can be found in Hutchins *et al.* (2005); Hutchins & Maru-

sic (2007); Adrian (2007); Elsinga *et al.* (2010); Dennis & Nickels (2011a,b); Gao (2011).

Previous studies by Tomkins (2001); Jacobi & McKeon (2011); Guala *et al.* (2012) have demonstrated profound effects that relatively small scale perturbations can make on the flow. Effects caused by many types of obstacles have been investigated, (e.g. Sakamoto & Arie, 1983; Schofield & Logan, 1988; Tomkins, 2001; Guala *et al.*, 2012). The current study will focus on the perturbation effects of a single spanwise array of cylinders with varying array spacing, due to the simplicity of the geometry. The cylinders are short compared with the boundary layer thickness, extending only through the logarithmic region.

Previous work has shown that a finite wall-mounted cylinder generates a complicated wake structure including tip vortices formed at the free end, Kármán vortices extending along most of the height (comparable to those downstream of infinite-length cylinders), and a horseshoe vortex system near the base (Williamson, 1996; Simpson, 2001). For individual cylinders, three parameters have been found to influence the wake flow significantly: the aspect ratio AR (Sumner *et al.*, 2004), the cylinder height with respect to the boundary layer thickness, H/δ (Sakamoto & Arie, 1983; Park & Lee, 2002; Hain *et al.*, 2008), and the condition of the incoming boundary layer, laminar or turbulent (Wang *et al.*, 2006). The current study considers cylinders of $AR=4$, $H/\delta=0.2$ ($H^+=500$) in a turbulent boundary layer.

A recent study by Pujals *et al.* (2010) investigated the effect of a single array of cylinders in a turbulent boundary layer at $Re_\tau=370$, with $H/\delta=0.8$ and constant cylinder spacing of $4D$ for several combinations of cylinder diameter and center-to-center distance. Based on the amplitude of spanwise variations in the streamwise velocity, they concluded that the streamwise development of the amplitude would be the same for a constant spacing normalized by the cylinder diameter D .

More recently, Ryan *et al.* (2011a) used Hot Wire Anemometry to probe the flow behind a single array of wall mounted cylinders with $AR=1.5$ in a turbulent boundary layer at $Re_\tau=1200$. The cylinder height was $H/\delta=0.15$ ($H^+=150$) such that they extended to the top of the log layer. Array spacings were 0.25δ and 0.5δ respectively, and

August 28 - 30, 2013 Poitiers, France

Table 1. Turbulent boundary layer parameters 6m downstream of the trip, as determined by Gao (2011).

Re_θ	Re_τ	U_∞ (m/s)	δ (mm)	u_τ (m/s)
6200	2500	0.508	125.5	0.0198

the results showed delay in cylinder wake interactions with increased spacing. Later, Ortiz-Dueñas *et al.* (2011) performed PIV and V3V measurements in a turbulent boundary layer at $Re_\tau=2500$ perturbed by a cylinder array of $AR=4$, $H/\delta=0.2$ ($H^+=500$). Cylinder spacings of 0.2δ and 0.4δ were considered, and the authors concluded that the 0.4δ spaced array produced relatively stable downstream structures while the 0.2δ case yielded rapid pairing of wake structures as well as greater disorganization of individual eddies downstream.

The current study extended the previous work by Ortiz-Dueñas *et al.* (2011) and Ryan (2011b) to larger cylinder spacings and greater streamwise distances to understand the development and stability of various spanwise modes. The impact of instantaneous initial flow conditions on the downstream development was also considered.

EXPERIMENTAL FACILITY AND METHODS

All experiments were conducted in a closed-return water channel with $Re_\tau=2500$ near the cylinder array location. The test section, which has length 8m and span 1.22m, was filled to a depth of 0.39m while running under steady conditions. A 3mm diameter stainless steel trip was mounted on the bottom wall in the beginning of the test section, and the measurement domain started $\sim 6m$ downstream. The flow parameters measured at this location are given in table 1.

A single spanwise array of stainless steel cylinders with aspect ratio $AR=4$ and height ($H/\delta=0.2$, $H^+=500$) was mounted on the bottom surface of the water channel 6m downstream of the trip. In the remainder of the paper, this location is defined as the origin of the x -axis. Spanwise and wall-normal directions are designated by y and z respectively. Four cylinder spacings were considered: 0.2δ , 0.4δ , 0.6δ and 0.8δ .

The particle image velocimetry method was used for all experiments. Beams from a Spectra Physics dual-head Nd:YAG laser (pulse energy=370mJ/pulse) were formed into overlapping sheets approximately 1mm thick and 15mm ($\tau^+=300$) above the wall. This height was chosen based on V3V measurements by Ryan (2011b), as a location of strong average wall normal velocity downstream of the cylinder array. Two 12-bit TSI PowerView 4MP Plus cameras with 2048×2048 pixels were used with Nikon Micro-Nikkor 60mm lenses. Both cameras were equipped with Scheimpflug adapters for quality imaging. The flow was seeded with silver coated hollow glass spheres from Potters Industries LLC, with a mean diameter of $16\mu m$ (diameter range of $6-25\mu m$).

Two types of measurements were performed: one based on acquiring data at fixed streamwise locations, and the other based on traversing the cameras and laser sheet at the local mean convection velocity. For fixed location measurements, both stereoscopic PIV and planar PIV were performed, referred to as SPIV and PPIV respectively. For SPIV experiments, the FOV was approximately $1.1\delta \times 1.1\delta$. For PPIV measurements, the spanwise FOV was increased to 1.9δ by minimizing the FOV overlap between the two

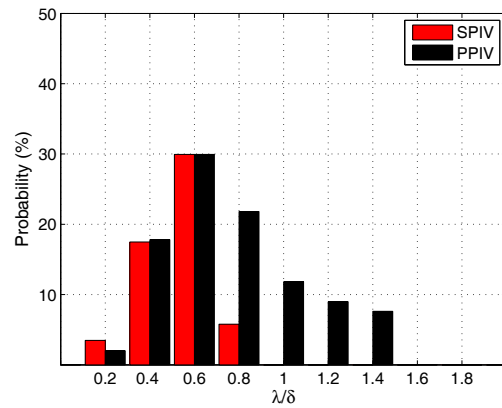


Figure 1. Distribution of dominant spanwise scales for unperturbed flow using SPIV (red) and PPIV (black). The SPIV probability scale is normalized to match the probability of the 0.6δ mode in PPIV.

cameras. This was necessary to observe and quantify spanwise variations for the larger array spacings.

Based on the traversing system mounted on top of the channel and the stereoscopic-PIV arrangement, a method referred to as flying PIV (FPIV) was employed to track the flow evolution in specific runs. For all FPIV experiments, data were acquired over a streamwise range of $-2 < x/\delta < 7$ so that the conditions approaching the cylinder array could be documented. The traversing speed (0.37m/s) was set based on the mean velocity at the measurement height in the unperturbed (no cylinder) case.

Velocity fields acquired at fixed measurement locations were analyzed using a Fourier transform method to determine the dominant mode of spanwise variation in streamwise velocity. Details of the method can be found in Zheng (2013). Figure 1 shows results for the unperturbed flow based on the SPIV and PPIV fields of view. The SPIV results are normalized to match the most dominant 0.6δ mode found by PPIV. This dominant scale is comparable to previous results by Hutchins *et al.* (2005). Based on this normalization, the components smaller than 0.6δ mode agree very well. Note, however, that the 0.8δ mode is not captured accurately by the smaller spanwise FOV in the SPIV measurements. Therefore, the PPIV data is used to discuss the 0.8δ and larger modes and any modes beyond 1.4δ are not considered as they are underestimated in the PPIV data.

The statistical uncertainty of the averaged results was estimated as 0.60%, 0.54% and 0.73% of U_∞ for U , V and W components respectively in SPIV, and 1.77% and 1.30% of U_∞ , for U and V component respectively in PPIV.

RESULTS

Averaged Results

Averaged streamwise velocity fields downstream of all four array spacings are plotted in figures 2 and 3. All four cases exhibit a similar pattern in that the wakes of slow moving fluid behind each cylinder appear to split symmetrically. For the 0.2δ spacing case, neighboring split wakes merge into new slow moving regions already at $x/\delta=0.5$ (with $x/\delta=0$ representing the cylinder location). The new slow moving regions are located in the streamwise wall-normal plane midway between neighboring cylinders, henceforth called the mid-spacing location. These slow moving regions persist until $x/\delta=2$ before they disappear. Beyond that location, the streamwise velocity appears uni-

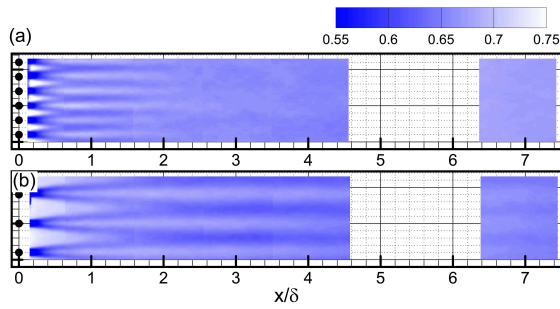


Figure 2. Averaged streamwise velocity field of (a) 0.2δ case and (b) 0.4δ case, normalized by $U_\infty=0.508\text{m/s}$ (blue is slow, white is fast). Spatial variables are normalized by $\delta=125.5\text{mm}$. Bold ticks on y-axis are separated by 0.5δ .

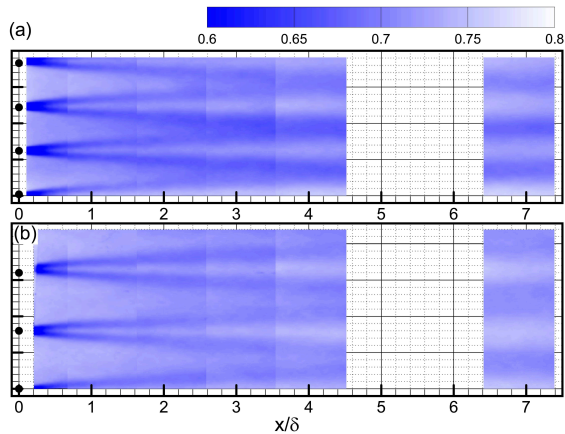


Figure 3. Averaged streamwise velocity field of (a) 0.6δ case and (b) 0.8δ case, normalized by $U_\infty=0.508\text{m/s}$ (blue is slow, white is fast). Spatial variables are normalized by $\delta=125.5\text{mm}$. Bold ticks on y-axis are separated by 0.5δ .

form across the span, and its magnitude increases gradually until it nearly matches the unperturbed value at $x/\delta=7.4$.

For the 0.4δ spacing in figure 2(b), the merging of the split wakes is delayed until $x/\delta=2$, and the resulting slow moving regions persist through the rest of the measurement domain although the amplitude of spanwise variation is considerably damped by $x/\delta=7.4$. Thus, the scale of the perturbation is better preserved than in the 0.2δ spacing case. These results are consistent with earlier results by Ortiz-Dueñas *et al.* (2011) and Ryan (2011b).

The 0.6δ and 0.8δ spacing cases in 3 show increasing delays in the streamwise location of wake merging. Note that the contour levels are different from those in figure 2 as the larger cylinder spacings lead to smaller velocity deficits. For 0.6δ spacing, the wake merging occurs at $x/\delta=3.5$, while for 0.8δ spacing, the merging appears to occur near $x/\delta=5$. The spanwise variations of streamwise velocity persist to $x/\delta=7.4$ in both cases. The amplitude of the variations was strongest for the 0.6δ spacing. Thus, it appears that 0.6δ spacing yields the most stable behavior as might be expected given that it is the most dominant spanwise scale in the unperturbed flow (see figure 1).

Figure 4 shows a sample plot of averaged wall-normal velocity obtained by SPIV. In all cases examined, a significant downwash was observed downstream of each cylinder. The downwash patterns, which did not shift in the spanwise direction, lasted longer as cylinder spacing was increased. In the 0.6δ case shown, the downwash lasted throughout the measurement domain. In general, this downwash behavior was related to tip vortices observed by Ryan (2011b)

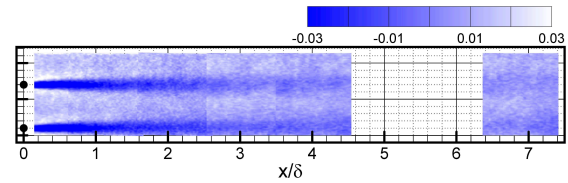


Figure 4. Averaged wall-normal velocity field of 0.6δ case, normalized by $U_\infty=0.508\text{m/s}$ (blue is towards the wall). Spatial variables are normalized by $\delta=125.5\text{mm}$. Bold ticks on y-axis are separated by 0.5δ .

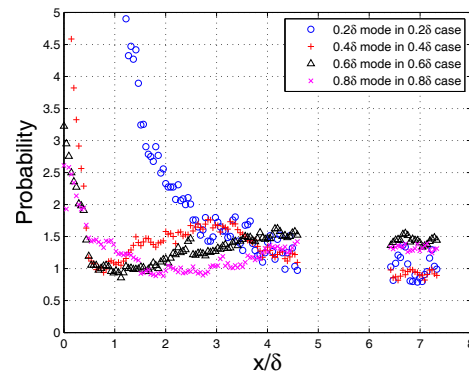


Figure 5. Streamwise development of spanwise perturbation scales. Normalized probability=1 means the percentage of the scale equals that in the unperturbed case.

that brought faster moving fluid from above the cylinders down toward the measurement plane, such that fast-moving regions then developed downstream of each cylinder.

Spanwise Scales

To compare the persistence of perturbations among the cases, the probability of the characteristic mode (the mode matching the perturbation scale) as most dominant in a given field was plotted vs. streamwise location. (see figure 5). Each probability was normalized by the corresponding value for unperturbed flow. A probability of 1 thus means that the characteristic scale is dominant as often as it is in the unperturbed case. The 0.2δ curve starts at a large value because its probability is small in the unperturbed case. It drops continuously with increasing x , reaching a value of 1.5 at about $x/\delta=3$ and a value near 1 by $x/\delta=4.5$. The 0.4δ curve, however, first drops to near 1 at $x/\delta=1$ (where the average wakes are splitting) and then rises to 1.5 at $x/\delta=3$ (where the split wakes have merged) before dropping back to about 1 at the end of the domain. The 0.6 and 0.8δ curves exhibit similar behavior related to and corresponding with the streamwise locations of wake splitting, then merging. In the far field ($x/\delta=6.4-7.4$), we can see a clear difference in probability of the various characteristic modes. The characteristic modes in the 0.2 and 0.4δ cases match the probabilities of the same modes in the unperturbed case. By contrast, the characteristic modes for both 0.6 and 0.8δ cases are more probable than in the unperturbed case, with values of 1.45 and 1.32 respectively. The 0.6δ case thus appears to be the most well preserved in the downstream flow, which is consistent with the behavior observed in the averaged results.

Flying PIV Results

The flying PIV method provided a means to track and observe the evolution of packet-like structures in both the unperturbed and perturbed flows. In the unperturbed flow,

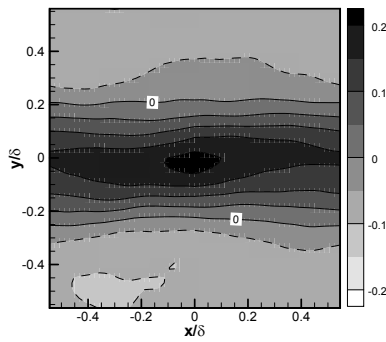


Figure 6. Cross correlation of the first and last frame of streamwise velocity field averaged over 40 runs for the unperturbed case.

distinct packets were observed frequently as identified by long LMRs surrounded by counter-rotating swirling structures and containing discrete Q2 Reynolds stress events. Very frequently, these packets persisted over a streamwise range greater than 9δ . The spanwise spacing between the LMRs was observed to vary over the range of $0.4-0.7\delta$, due to spanwise inclinations also observed in many previous studies. Sometimes, the spanwise inclinations were observed to result from slow rotation of the LMRs about a wall-normal axis.

Figure 6 shows the plot resulting from correlating the first and last frame of the streamwise velocity fields obtained in each run, averaged over 40 runs. Note that the fields are well correlated over the streamwise range, and that the zero contour lines (marked by white patches) indicate the width of the LMRs to be approximately 0.2δ , which is consistent with observations by Tomkins & Adrian (2003) and Hutchins & Marusic (2007). It is also interesting that the strongest contours show a diamond-shape which could be caused partly by spanwise rotation of LMRs.

Figure 7 gives a sample FPIV run with the 0.2δ array in place. Two distinct packets are observed in the incoming flow, identified by the well aligned swirls on both sides of the long LMRs. Immediately downstream of the cylinders, the streamwise velocity is significantly decreased, and individual wake structures interact with their neighbors. Consequently, the number of swirl structures increases, and their sizes become more diverse at this measurement location.

The incoming vortex packets appear to be broken down, and the resulting individual vortices are distributed across the span so that the flow appears very disorganized until approximately $x/\delta=2$. Then, the swirling structures start to reorganize towards a distribution similar to that in the incoming flow, i.e. beyond $x/\delta=2$, two independent LMRs accompanied by swirling zones of appropriate sign are again observed, and their spanwise spacing and location are similar to those of the upstream packets. This behavior is observed frequently in the 0.2δ case, which suggests that the cylinder array only perturbs part of the existing packets, and the remaining organization in the outer layer significantly affects the development of the flow downstream. This concept is congruent with the idea of Hutchins & Marusic (2007) that packets in the outer region make a significant imprint on the near wall region.

Figure 8 shows the result for the 0.2δ case for the same cross correlation described above. The region of highest correlation is elongated in the streamwise direction compared to the unperturbed case, suggesting first that the packet structure persists in spite of the perturbation and second that the spanwise movement of the existing packets is

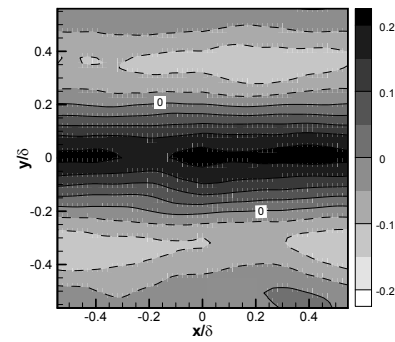


Figure 8. Cross correlation of the first and last frame of streamwise velocity field averaged over 40 runs for the 0.2δ case.

decreased compared with the unperturbed case. The spanwise contour variation is also different in that the negative lobes become more prominent. This feature also could result from decreased spanwise movement or rotation of the approaching LMRs which are surrounded by high momentum regions. The zero value contours suggest a slightly narrower width than in the unperturbed case.

When the cylinder spacing increases beyond 0.2δ , the instantaneous downstream flow organization depends more on the upstream flow conditions. After a thorough examination of many runs, three scenarios were proposed to explain the wake-packet interactions. In the first scenario, no distinct packets were observed in the incoming flow, and individual cylinder wakes merged or paired into new slow moving regions at spanwise locations midway between the cylinders. In the second scenario, packets in the incoming flow passed between neighboring cylinders and attracted the nearest wake so that the existing LMRs were strengthened and remained coherent in the mid-spacing locations. In the third scenario, the incoming packets impinged directly on the cylinders. The packets were enhanced by the coincident cylinder wakes before shifting gradually toward the mid-spacing locations. Scenario I occurs $\sim 12\%$ of the time, while II and III make up the remainder. Selected runs of the 0.6δ case are shown in figure 9 for each scenario.

Figure 9(a) represents the first scenario where no distinct packets are present in the incoming flow. This is based on the rather disorganized distribution of swirling structures. Individual wakes downstream of the cylinders appear very unstable and bend in either the positive or negative spanwise direction causing significant interactions between neighboring wakes. An example of the spanwise movement is observed at $x/\delta=1$ based on the tilting of like-signed groups of swirls. At $x/\delta=2$, two neighboring wakes merge into a distinct LMR in the mid-spacing location which persists throughout the measurement field. In this case, the spanwise movement of the wakes is initiated by the tip downwash effects, as faster moving fluid is connected downward from above the cylinders forcing the wake structures to move aside. This feature was supported by Q4 Reynolds stress events immediately neighboring individual cylinder wakes.

In figure 9(b), a packet in the incoming flow passes between neighboring cylinders. In this case, the cylinder wakes interact with the packet immediately downstream of the array. The swirl structures showed clear evidence of the wakes merging laterally into the packet. In this scenario, the LMR settled at the mid-spacing location and remained coherent throughout the measurement domain with no further strong spanwise interactions. This wake-packet

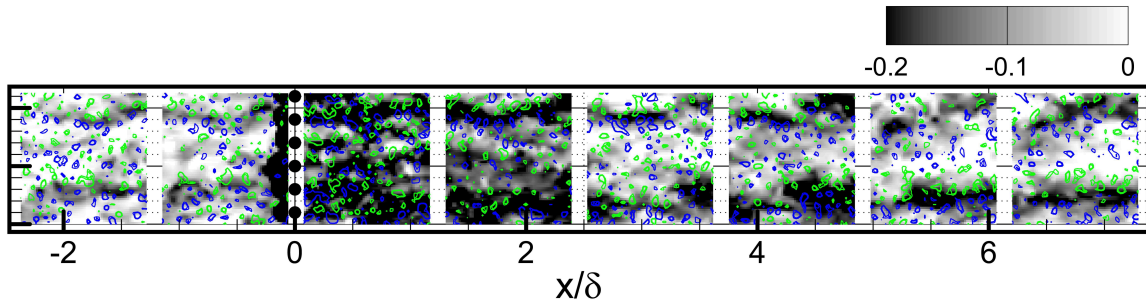


Figure 7. Sample run of 0.2δ spacing case. Contour map shows streamwise velocity relative to $\bar{U}=0.37\text{m/s}$ normalized by $U_\infty=0.508\text{m/s}$. The 2D swirling strength is marked by contour lines (blue: $\lambda_{ci}>0.6$, green: $\lambda_{ci}<-0.6$, signed by ω_z). Bold ticks on y-axis are separated by 0.5δ . [Zoom in for better resolution.]

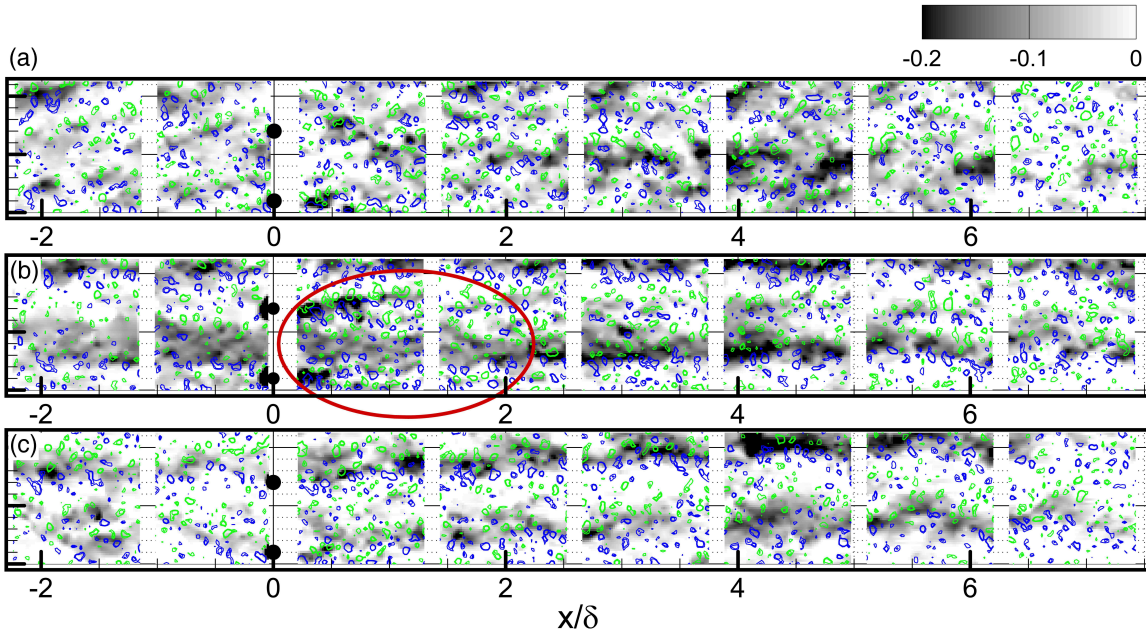


Figure 9. Select runs of 0.6δ spacing case representing the three scenarios of wake-packet interaction. Contour map shows the relative streamwise velocity to $\bar{U}=0.37\text{m/s}$ normalized by $U_\infty=0.508\text{m/s}$. The 2D swirling strength are given in contour lines (blue: $\lambda_{ci}>0.6$, green: $\lambda_{ci}<-0.6$, signed by ω_z). Bold ticks on y-axis are separated by 0.5δ . The red circle in (b) shows merging of the cylinder wake into the packet. [Zoom in for better resolution.]

merging, which could be aided by downwash, was observed frequently under this scenario.

Finally, figure 9(c) illustrates the third scenario whereby packets impinge directly on the cylinders. The diverging pattern of blue and green swirls just upstream of the upper cylinder suggests that the vortex packet is indeed obstructed and slowed by the cylinder. Downstream of the cylinder array, the two packets are enhanced by the wakes as the population of (conventional) streamwise-aligned swirls increases. No spanwise interaction is observed between the neighboring packets, and they move gradually toward the mid-spacing location. The spanwise spacing between them remains about 0.6δ throughout the measurement domain. The spanwise movement of the enhanced packets in this case was induced by downwash directly behind each cylinder, as observed in separate plots of Q4 Reynolds stress events (see Zheng, 2013).

Since the 0.4δ cylinder array had a spacing different from the most dominant spanwise scale of 0.6δ in the unperturbed (incoming) flow, a mixed scenario (II and III) was frequently observed for that array, resulting in more disorganization of the downstream flow structures due to the different wake-packet interaction schemes for each scenario. For the 0.6δ array, however, the relative packet-to-cylinder

position was more likely to be the same for neighboring packets; thence either scenario II or III would occur and dominate the downstream flow. Consequently, the wake-packet interactions and development of neighboring packets was better organized in the downstream flow, helping explain the enhanced flow stability in the 0.6δ case.

CONCLUSIONS

Particle image velocimetry measurements were performed to study the perturbations caused by a single spanwise array of cylinders immersed in the logarithmic region of a turbulent boundary layer. In the unperturbed flow, features of strong coherent packets were observed that persisted over 9δ in the streamwise direction. Interrogation of streamwise velocity variations in the spanwise direction revealed a dominant spanwise scale of 0.6δ which can be interpreted as a dominant spanwise packet spacing.

In the 0.2δ array case, the downstream flow recovered relatively rapidly from the perturbation. The recovery applied not only to the average streamwise velocity but also to the dominant spanwise scales and the upstream packet structures. The flying PIV measurements suggested that packet organization in the outer layer persisted through the

August 28 - 30, 2013 Poitiers, France

perturbation and communicated in to reestablish itself in the logarithmic region.

For arrays with larger cylinder spacing, three scenarios of wake-packet interactions were observed. Downwash downstream of cylinder tips acted to destabilize the corresponding cylinder wakes, displacing them in either spanwise direction. Depending on the scenario, this encouraged either formation of new packets in the midspan locations or migration of existing packets into the same locations. Packets passing close to a given cylinder tended to ingest the wake from that cylinder, potentially strengthening their existing organization. The 0.6δ array yielded the most stable organization of LMRs downstream which was not surprising as it matched the dominant spanwise scale in the unperturbed flow. At the end of the measurement domain (7.4δ downstream of the array), the Fourier analysis showed that the 0.6δ scale was still 45% more probable in the perturbed case than in the unperturbed case, suggesting a long-lasting effect.

Future work will include measurements with different cylinder heights as well as measurements at different wall-normal locations to examine further the importance of the downwash effects.

ACKNOWLEDGEMENTS

The authors gratefully acknowledge support from the U.S. National Science Foundation through Grant CBET-0933341.

REFERENCES

- Adrian, R. J. 2007 Hairpin vortex organization in wall turbulence. *Phys. Fluids* **19** (4).
- Adrian, R. J., Meinhart, C. D. & Tomkins, C. D. 2000 Vortex organization in the outer region of the turbulent boundary layer. *J. Fluid Mech.* **422**, 1–54.
- Dennis, D. J. C. & Nickels, T. B. 2011a Experimental measurement of large-scale three-dimensional structures in a turbulent boundary layer. part 1. vortex packets. *J. Fluid Mech.* **673**, 180–217.
- Dennis, D. J. C. & Nickels, T. B. 2011b Experimental measurement of large-scale three-dimensional structures in a turbulent boundary layer. part 2. long structures. *J. Fluid Mech.* **673**, 218–244.
- Elsinga, G. E., Adrian, R. J., van Oudheusden, B. W. & Scarano, F. 2010 Three-dimensional vortex organization in a high-reynolds-number supersonic turbulent boundary layer. *J. Fluid Mech.* **644**, 35–60.
- Elsinga, G. E., Kuik, D. J., van Oudheusden, B. W. & Scarano, F. 2007 Investigation of the three-dimensional coherent structures in a turbulent boundary layer with Tomographic-PIV. In *45th AIAA Aerospace Sciences Meeting and Exhibit*. Reno, NV, USA.
- Ganapathisubramani, B., Longmire, E. K. & Marusic, I. 2003 Characteristics of vortex packets in turbulent boundary layers. *J. Fluid Mech.* **478**, 35–46.
- Gao, Q. 2011 Evolution of eddies and packets in turbulent boundary layers. PhD thesis, University of Minnesota.
- Guala, M., Tomkins, C. D., Christensen, K. T. & Adrian, R. J. 2012 Vortex organization in a turbulent boundary layer overlying sparse roughness elements. *J. Hydraulic Research* **50** (5), 465–481.
- Hain, R., Kähler, C. J. & Michaelis, D. 2008 Tomographic and time resolved PIV measurements on a finite cylinder mounted on a flat plate. *Exp. Fluids* **45**, 715–724.
- Hutchins, N., Ganapathisubramani, B. & Marusic, I. 2005 Spanwise periodicity and the existence of very large scale coherence in turbulent boundary layers. *Proc. Turbulence and Shear Flow Phenomena IV*.
- Hutchins, N. & Marusic, I. 2007 Evidence of very long meandering features in the logarithmic region of turbulent boundary layers. *J. Fluid Mech.* **579**, 1–28.
- Jacobi, I. & McKeon, B. J. 2011 New perspectives on the impulsive roughness-perturbation of a turbulent boundary layer. *J. Fluid Mech.* **677**, 179–203.
- Lee, J. H. & Sung, H. J. 2011 Very-large-scale motions in a turbulent boundary layer. *J. Fluid Mech.* **673**, 80–120.
- Ortiz-Dueñas, C., Ryan, M. D. & Longmire, E. K. 2011 Modification of turbulent boundary layer structure using immersed wall-mounted cylinders. In *Proc. Turbulence and Shear Flow Phenomena VII*. Ottawa, Canada.
- Park, C. W. & Lee, S. J. 2002 Flow structure around a finite circular cylinder embedded in various atmospheric boundary layers. *Fluid Dynamics Research* **30** (4), 197–215.
- Pujals, G., Cossu, C. & Depardon, S. 2010 Forcing large-scale coherent streaks in a zero-pressure-gradient turbulent boundary layer. *J. Turbulence* **11** (25), 1–13.
- Ryan, M. D. 2011b Planar and volumetric measurements downstream of cylinders immersed in a turbulent boundary layer. Master's thesis, University of Minnesota.
- Ryan, M. D., Ortiz-Duenas, C. & Longmire, E. K. 2011a Effects of simple wall-mounted cylinder arrangements on a turbulent boundary layer. *J. AIAA* **49** (10), 2210–2220.
- Sakamoto, H. & Arie, M. 1983 Vortex shedding from a rectangular prism and a circular-cylinder placed vertically in a turbulent boundary-layer. *J. Fluid Mech.* **126** (JAN), 147–165.
- Schofield, W. H. & Logan, E. 1988 Viscous flow around two and three dimensional wall mounted obstacles. In *1st AIAA, ASME, SIAM, and APS, National Fluid Dynamics Congress*, pp. 1742–1748. Cincinnati, OH, USA.
- Simpson, R. L. 2001 Junction flows. *Annu. Rev. Fluid Mech.* **33**, 415–443.
- Sumner, D., Heseltine, J. L. & Dansereau, O. J. P. 2004 Wake structure of a finite circular cylinder of small aspect ratio. *Exp. Fluids* **37** (5), 720–730.
- Tomkins, C. D. 2001 The structure of turbulence over smooth and rough walls. PhD thesis, University of Illinois at Urbana-Champaign.
- Tomkins, C. D. & Adrian, R. J. 2003 Spanwise structure and scale growth in turbulent boundary layers. *J. Fluid Mech.* **490**, 37–74.
- Wang, H. F., Zhou, Y., Chan, C. K. & Lam, K. S. 2006 Effect of initial conditions on interaction between a boundary layer and a wall-mounted finite-length-cylinder wake. *Phys. Fluids* **18** (6), 1–12.
- Williamson, C. H. K. 1996 Vortex dynamics in the cylinder wake. *Annu. Rev. Fluid Mech.* **28** (1), 477–539.
- Zheng, S. 2013 Perturbing spanwise modes in turbulent boundary layers. Master's thesis, University of Minnesota.